Journal of the Korean Chemical Society
2019, *Vol. 63, No. 6*
Printed in the Republic of Korea
https://doi.org/10.5012/jkcs.2019.63.6.453

Sol-Gel Synthesis, Crystal Structure, Magnetic and Optical Properties in $ZnCo_2O_3$ Oxide

Bidhu Bhusan Das* and Bittesh Barman

Department of Chemistry, Functional Materials Chemistry Laboratory, Pondicherry University, Puducherry-605014, India.
**E-mail: bidhubnds@gmail.com*

(Received May 5, 2019; Accepted August 13, 2019)

ABSTRACT. Synthesis of $ZnCo_2O_3$ oxide is performed by sol-gel method via nitrate-citrate route. Powder X-ray diffraction (XRD) study shows monoclinic unit cell having lattice parameters: a = 5.721(1) Å, b = 8.073(2) Å, c = 5.670(1) Å, β = 93.221(8)°, space group $P_{2/m}$ and Z = 4. Average crystallite sizes determined by Scherrer equation are the range ~14-32 nm, whereas SEM micrographs show nano-micro meter size particles formed in $ZnCo_2O_3$. Endothermic peak at ~798 K in the Differential scanning calorimetric (DSC) trace without weight loss could be due to structural transformation and the endothermic peak ~1143 K with weight loss is due to reversible loss of O_2 in air atmosphere. Energy Dispersive X-ray (EDX) analysis profile shows the presence of elements Zn, Co and O which indicates the purity of the sample. Magnetic measurements in the range of +12 kOe to -12 kOe at 10 K, 77 K, 120 K and at 300 K by PPMS-II Physical Property Measurement System (PPMS) shows hysteresis loops having very low values of the coercivity and retentivity which indicates the weakly ferromagnetic nature of the oxide. Observed X-band EPR isotropic lineshapes at 300 K and 77 K show positive g-shift at g_{iso} ~2.230 and g_{iso} ~2.217, respectively which is in agreement with the presence of paramagnetic site $Co^{2+}(3d^7)$ in the oxide. DC conductivity value of 2.875 x10^{-8} S/cm indicates very weakly semiconducting nature of $ZnCo_2O_3$ at 300 K. DRS absorption bands ~357 nm, ~572 nm, ~619 nm and ~654 nm are due to the d-d transitions $^4T_{1g}(^4F)\rightarrow{}^2E_g(^2G)$, $^4T_{1g}(^4F)\rightarrow{}^4T_{1g}(^4P)$, $^4T_{1g}(^4F)\rightarrow{}^4A_{2g}(^4F)$, $^4T_{1g}(^4F)\rightarrow{}^4T_{2g}(^4F)$, respectively in octahedral ligand field around Co^{2+} ions. Direct band gap energy, E_g~ 1.5 eV in the oxide is obtained by extrapolating the linear part of the Tauc plot to the energy axis indicates fairly strong semiconducting nature of $ZnCo_2O_3$.

Key words: Sol-gel synthesis, Powder X-ray diffraction, Magnetic properties, Electron paramagnetic resonance

INTRODUCTION

Nano-oxide materials are of great interest in research in these decades due to their unique electronic, optical, thermal and magnetic properties[1–7] and applications in the areas such as photocatalyst[8–10] and electrocatalyst.[11,12] Among the Nano-oxide materials, special attention is also focused on research in complex oxides especially containing transition metals[13,14] (TM) due to their unusual electronic and magnetic properties with potential applications in the next generation magnetic recording and optical memory devices.[15–17] Apart from the usual solid state reactions and related techniques, these days several wet chemical methods have also been used to the synthesis of nano-oxide materials. The methods like hydrothermal, co-precipitation, sol-gel, combustion and spray pyrolysis are mostly used.[9] Among these, sol-gel synthesis is relatively a more effective method to synthesize nano-oxide materials due to low-processing cost, energy efficiency, and easy to produce homogeneous nanosize powder at multiscale.[18–20] In this paper, we report our investigations on $ZnCo_2O_3$ complex oxide, prepared by sol-gel synthesis, using various structure sensitive techniques such as: powder XRD, DSC, thermogravimetric analysis (TGA), scanning electron microscopy (SEM), energy-dispersive X-ray (EDX) analysis, magnetic measurements by PPMS, electron paramagnetic resonance (EPR) spectroscopy, AC electrical conductivity measurements, diffuse reflectance spectroscopy and density measurements.

EXPERIMENTAL

Sol-gel synthesis of $ZnCo_2O_3$ complex oxide is performed via nitrate-citrate precursor route.[21] Calculated amounts of $Zn(NO_3)_2$ and $Co(NO_3)_2$ are dissolved in distill water to prepare 0.1 M solution of each which are then mixed together and stirred for 30 min at ~323 K to form the sol. Then 30 ml of 1.5 M citric acid solution is added to the sol and the pH is adjusted to ~2.0 to ensure smaller particle sizes.[22] The sol is air dried by continuous stirring for ~90 h at ~323 K to form the gel. The gel is decomposed to powder at ~393 K which is then calcined at ~893 K for 8 h followed by sintering at ~1223 K for 10 h and air quenching to obtain black

fine powder.

Powder XRD pattern of the sample is recorded on an X'pert powder X-ray diffractometer (PAN ANALYTICAL make) with scan rate 2° per minute in range 10°-80° in 2θ. Monochromatic Cu K_α radiation (λ~1.5406 Å) is used as the X-ray source with power of 40 kV/30 mA. SEM images and EDX profiles are recorded by using JEOL, JSM 6390 instrument. DSC and TGA data are recorded on a Thermogravimetric analyzer (TA instruments, Q600 SDT and Q20 DSC) in the range 298 -1273 K. Magnetic measurements are done using Quantum Design Model: PPMS-II Physical Property Measurement System (PPMS). Magnetic moments of the sample in emu/g are obtained at 10 K, 77 K, 120 K and 320 K by applying magnetic fields in the cyclic range -12 kOe to +12 kOe. X-band EPR spectral measurements at 300 K and 77 K are done with a JEOL JES200 ESR spectrometer with 100 kHz magnetic field modulation. AC electrical conductivity data at 300 K are recorded with an Impedance Spectroscopic Analyzer (Novocontrol) in the frequency range 50 mHz to 10 MHz. Ultraviolet-visible diffuse reflectance spectroscopic (UV-Vis DRS) measurements are taken over the range 200-800 nm using a Varian model 5000 UV-Vis-NIR spectrophotometer. Density of the sample is determined by liquid displacement method using dibutylphthalate as an immersion liquid (density 1.043 g/cc at 300 K).

RESULTS AND DISCUSSION

Fig. 1 shows the powder XRD pattern of $ZnCo_2O_3$ along with the indexed lattice planes. The XRD data are analyzed by the FullProf Suite (version 3.90) software package[23] to determine the unit cell parameters and indexing. The obtained cell parameters are: unit cell type monoclinic, a = 5.721(1) Å, b = 8.073(2) Å, c = 5.670(1) Å, β = 93.221(8)° and space group $P_{2/m}$. By the comparing the observed density value of 4.584 g/cc to that of the calculated density value 5.880 g/cc the value of Z is determined to be 4 for the unit cell structure. Using the Scherrer equation[24] the average crystallite sizes of the ordered (crystalline) domains, which may be smaller or equal to the particle size are found to be in the range ~14-32 nm. This indicates that the crystalline domains in the oxide are in nanometer range. However, the particle sizes of $ZnCo_2O_3$ could be ascertained from the SEM micrographs of the sample discussed shortly.

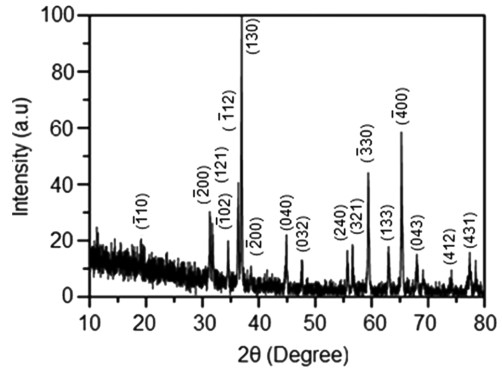

***Figure* 1.** Powder XRD pattern of $ZnCo_2O_3$ with indexed lattice planes.

The SEM micrographs at two different magnifications of two randomly selected particles of $ZnCo_2O_3$ are shown in *Fig.* 2(a-b), which show irregular micro structures comprising single or agglomerated particles with respect to the particle sizes and shapes in the sample. It may also be pointed out that the particle sizes vary in the nano-micro meter range, whereas the mean crystallite sizes in the oxide determined by Scherer equation are in the nanometer range. The representative EDX profile of the sample is shown in *Fig.* 3. EDX profile shows the presence of staring elements Zn, Co and O only indicating the purity of the sample.

Fig. 4 shows the DSC-TGA traces of $ZnCo_2O_3$ in the range of 298~1273 K. Endothermic peak at ~798 K in DSC trace without weight loss could be due to some structural phase transformation. Further at higher temperatures up to ~1123 K absence of any characteristic event in the DSC-

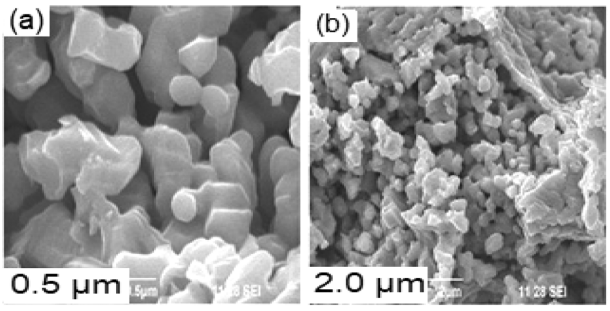

***Figure* 2.** (a)-(b) SEM micrographs of two particles of $ZnCo_2O_3$ at different magnifications.

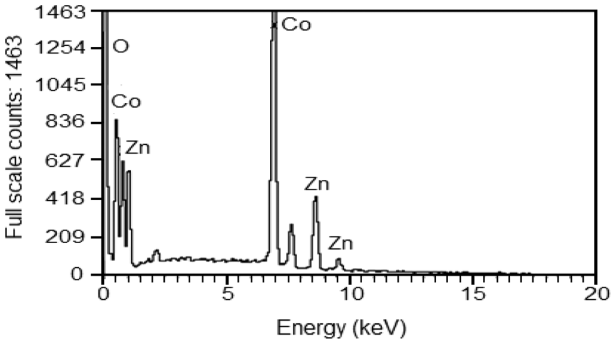

***Figure* 3.** EDX profile of $ZnCo_2O_3$.

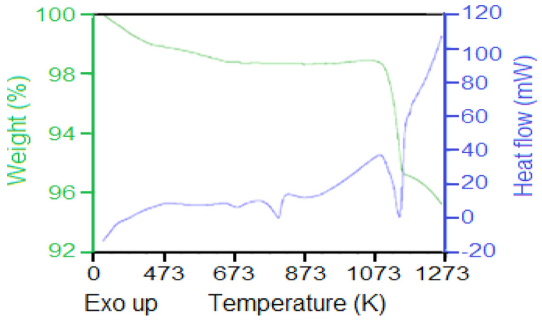

***Figure* 4.** DSC-TGA traces of $ZnCo_2O_3$ at air atmosphere in the range 298-1273 K.

TGA traces shows the thermal stability of the sample up to ~1123 K. Furthermore, weight loss in the sample ~1143 K could be attributed to the decomposition of the sample due to loss of oxygen. This fact is verified from the powder XRD pattern of the sample heated up to 1193 K in air atmosphere and cooled to room temperature which shows the same XRD pattern as that of the pattern before heating. This result indicates that the sample decomposes at ~1143 K reversibly according to the following reaction in air atmosphere:

$$4Co^{2+} + 4O^{2-} \rightleftharpoons 4Co^{+} + 2O^{2-} + O_2\uparrow \quad (1)$$

Fig. 5 shows the magnetic moment versus magnetic field plots of $ZnCo_2O_3$ in the range of +12 kOe to -12 kOe at 10 K, 77 K, 120 K and at 300 K along with the zoomed parts of the plots in the magnetic field range 0.10 kOe to -0.10 kOe (inset). The plots show apparently straight lines having no saturation magnetization up to the range of ±12 kOe. However, the inset plots show the formation of hysteresis loops having insignificant loop areas and very low values of the coercivity and retentivity (*Table* 1). Calculated values of the magnetic susceptibilities at the above temperatures are also found to be very low. This behaviour indicates the soft ferromagnetic nature of the sample in the temperature range studied.

Fig. 6 shows the observed X-band EPR lineshapes of $ZnCo_2O_3$ at 300 K and 77 K. All the EPR lineshapes of the sample at 300 K and 77 K are fairly broad and isotropic in nature without any hyperfine structures. The observed g_{iso}-values of the EPR lineshapes at 300 K and 77 K are ~2.230 and ~2.217, respectively. The observed positive g-shift in the oxide indicates Co^{2+} ($3d^7$, ^4F, S = 3/2) as the magnetic site in the oxide. The broad unresolved lineshapes are attributed mainly due to the rapid spin-lattice relaxation times of the Co^{2+} ($3d^7$) electrons in $ZnCo_2O_3$ oxide. The observed g_{iso}-values at 300 K and 77 K are not significantly different which indicates that the polyhedra containing the

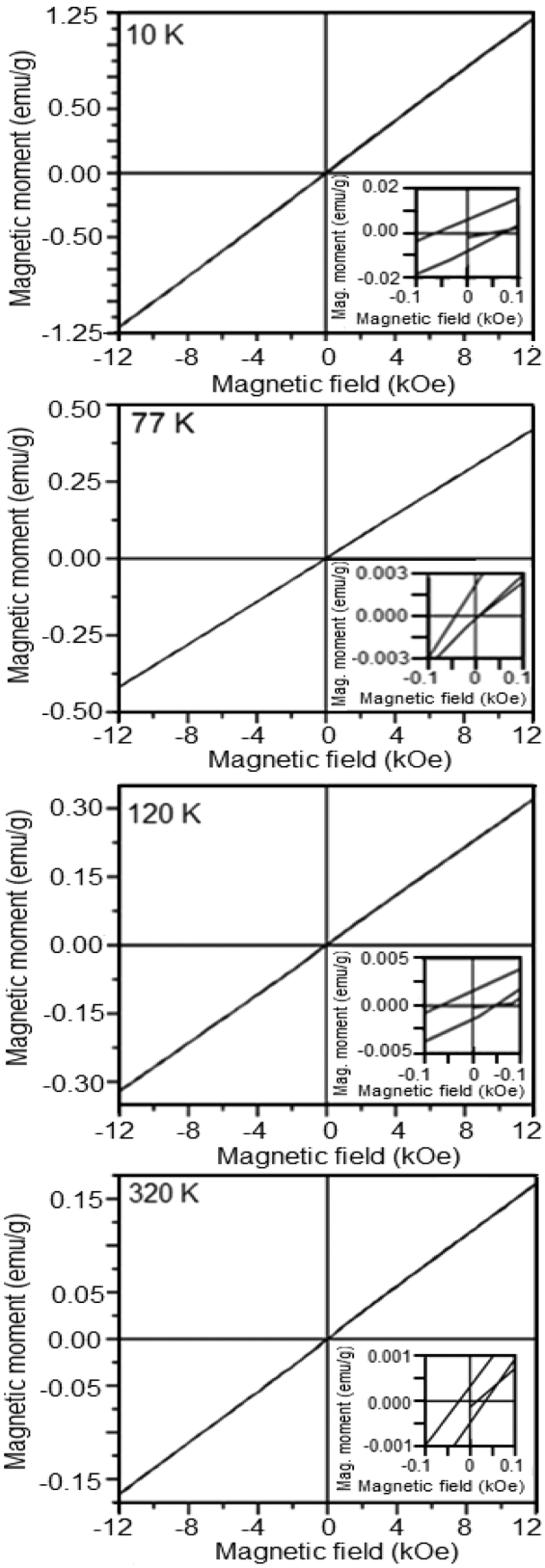

***Figure* 5.** Magnetic moment versus magnetic field plots at 10 K, 77 K, 120 K and 320 K of $ZnCo_2O_3$.

***Table* 1.** Observed values of coercivity (H_c), retentivity (M_R) and calculated magnetic susceptibility (χ) at 10 K, 77 K, 120 K, 320 K

Temperature (K)	H_c (Oe)	M_R (emu/g)	χ (emu/gOe)
10	66.25	0.0070	7.37×10^{-5}
77	25.43	0.0012	2.98×10^{-5}
120	56.75	0.0014	2.43×10^{-5}
320	29.93	0.0004	1.27×10^{-5}

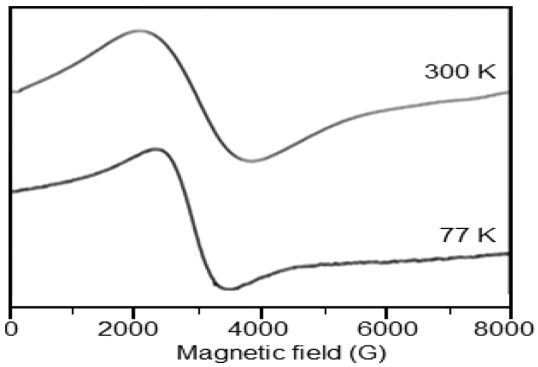

***Figure* 6.** EPR lineshapes of $ZnCo_2O_3$ at 300 K and 77K.

Co^{2+} sites are nearly the same in terms of size and symmetry in the range 300-77 K.

The complex AC electrical conductivity,[25,26] σ*, is given by,

$$\sigma^*(f) = \sigma'(f) + \sigma''(f) \quad (2)$$

where σ′ is the real part and σ″ is the imaginary part. The real part σ′ is called the AC conductivity. AC electrical conductivity, σ′, versus frequency plot (*Fig.* 7) of $ZnCo_2O_3$ at 300 K shows exponential increase in σ′ with increasing frequencies up to 10 MHz which indicates frequency dependent conductivity in $ZnCo_2O_3$. From extrapolation of the plot to zero Hz the DC conductivity of $ZnCo_2O_3$ is determined as 2.875×10^{-8} S/cm. This result shows very weakly

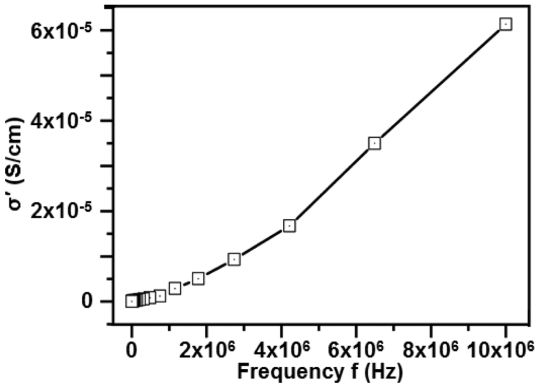

***Figure* 7.** AC electrical conductivity σ′ versus frequency plot of $ZnCo_2O_3$ at 300 K.

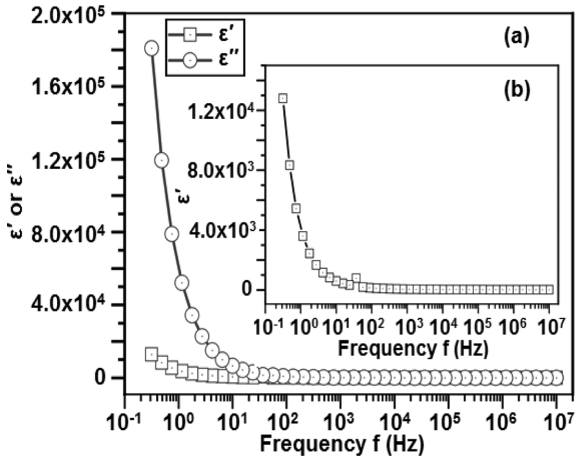

***Figure* 8.** Plots of dielectric constant, ε′, and dielectric loss factor, ε″, versus AC frequency of $ZnCo_2O_3$ at 300 K.

semiconducting nature of $ZnCo_2O_3$ at 300 K.

The complex dielectric function, ε*, is given by,

$$\varepsilon^* = \varepsilon' + i\varepsilon'' \quad (3)$$

where the real part ε′ is called the dielectric constant, and the imaginary part, ε″, is called the dielectric loss factor due to the conduction process. *Fig.* 8 shows the plots of ε′ and ε″ versus AC frequencies at 300 K. The plots show both ε′ and ε″ decrease exponentially with increasing AC frequencies up to 100 Hz and then remain plateau up to 10 MHz at very low values. The plots also show that the decrease in loss factor, ε″, is more rapid than ε′ with increasing frequencies up to ~100 Hz.

Fig. 9 shows the Ultraviolet-visible diffuse reflectance absorption spectrum of $ZnCo_2O_3$ at 300 K. The absorption bands ~ 357 nm, 572 nm, 619 nm and 654 nm are due to the d-d transitions $^4T_{1g}(^4F) \rightarrow {}^2E_g(^2G)$, $^4T_{1g}(^4F) \rightarrow {}^4T_{1g}(^4P)$, $^4T_{1g}(^4F) \rightarrow {}^4A_{2g}(^4F)$, $^4T_{1g}(^4F) \rightarrow {}^4T_{2g}(^4F)$, respectively of Co^{2+} ($3d^7$) ions in tetragonally distorted octahedral environment in the oxide matrix.[27] Furthermore, it can be mentioned that no

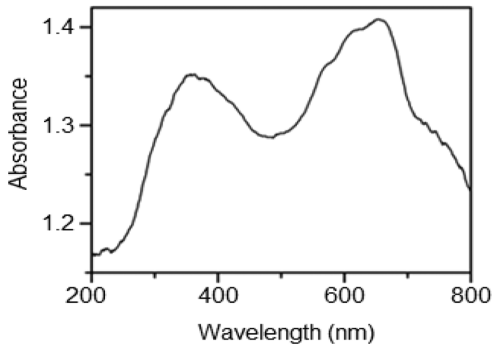

***Figure* 9.** DRS absorption spectrum of $ZnCo_2O_3$.

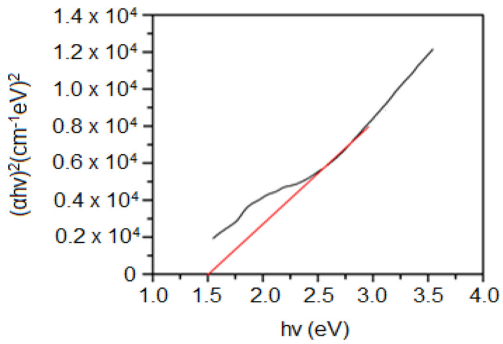

***Figure* 10.** Plot of $(\alpha h\nu)^2$ vs hν of $ZnCo_2O_3$ where α is the absorption coefficient, h, the Planck's constant and ν the frequency of light.

metal $-O^{2-}$ charge-transfer band[28] which normally appears in the range ~250-350 nm is observed for this oxide.

Fig. 10 shows the plot of $(\alpha h\nu)^2$ vs hν (Tauc plot[29]) of $ZnCo_2O_3$,obtained from the data in *Fig.* 9, where α is absorption coefficient. The direct band gap energy, E_g, of the sample is obtained by extrapolating the linear part of the plot to the photon energy axis. The obtained E_g value of 1.5 eV is in the range of values for semiconductors. However, it may be mentioned here that from our earlier discussion, the more reliable DC conductivity value of 2.875×10^{-8} S/cm indicates that the oxide $ZnCo_2O_3$ could be very weakly semiconductor at 300 K.

CONCLUSION

Single phase $ZnCo_2O_3$ is synthesized by sol-gel method via citrate route. Powder XRD studies show monoclinic unit cell having cell parameters: a = 5.721(1) Å, b = 8.073(2) Å, c = 5.670(1) Å, β = 93.221(8)°, space group $P_{2/m}$ and Z = 4. SEM micrographs show irregular micro structures of the particles. Average crystallite sizes ~14-32 nm show the formation of nanosize crystallites or ordered (crystalline) domains, and the SEM micrographs show the formation nano-micro meter size particles in $ZnCo_2O_3$. Magnetic moments data show the presence of hysteresis loops having very low loop areas which indicates soft ferromagnetic nature of the oxide at 10 K, 77 K, 120 K and 320 K. Observed EPR lineshapes of the oxide are broad and isotropic having g_{iso}- values ~2.230 and ~2.217 at 300 K and 77 K, respectively. AC electrical conductivity result shows frequency dependent conductivity at 300 K, and the obtained DC conductivity value of 2.875×10^{-8} S/cm indicates very weakly semiconducting nature of $ZnCo_2O_3$ at 300 K. DRS absorption bands ~ 357 nm, 572 nm, 619 nm and 654 nm are due to tetragonally distorted octahedral field around the Co^{2+} ($3d^7$) sites in $ZnCo_2O_3$. Direct band gap energy, E_g ~ 1.5 eV although indicates significant semiconducting nature, the more plausible DC conductivity value of ~2.875×10^{-8} S/cm indicates very weakly semiconducting nature of $ZnCo_2O_3$.

Acknowledgments. The authors thank SAIF IIT Madras for providing X-band EPR data at 300 K and 77 K and the CIF Pondicherry University, Pondicherry for the PPMS and rest of the data for this paper. And the publication cost of this paper was supported by the Korean Chemical Society.

REFERENCES

1. Duan, X. F.; Huang, Y.; Agarwal, R.; Lieber, C. M. *Nature* **2003**, *421*, 241.
2. Gudiksen, M.S.; Lauhon, L. J.; Wang J. F.; Smith, D. C.; Lieber, C. M. *Nature* **2002**, *415*, 617.
3. Hgfeldt, A.; Gratzel, M. *Chem. Rev.* **1995**, *95*, 49.
4. Duan, X. F.; Huang, Y.; Cui, Y.; Wang, J. F.; Lieber, C.M. *Nature* **2001**, *409*, 66.
5. Hu, J. G.; Odom, T. W.; Lieber, C.M. *Acc. Chem. Res.* **1999**, *32*, 435.
6. Yao, Z.; Postma, H. W. C.; Balents, L.; Dekker, C. *Nature* **1999**, *402*, 273.
7. Yang, P.; Lieber, C. M. *Science* **1996**, *273*, 1836.
8. Gowrishankar, M.; Babu, D. R.; Madeswaran, S. *J. Magn. Magn. Mater.* **2016**, *418*, 54.
9. Ramesh, S.; Ramaclus, J. V.; Mosquera, E.; Das, B. B. *RSC Adv.* **2016**, *6*, 6336.
10. Wei, W.; Cui, X.; Chen, W.; Ivey, D. G. *Chem. Soc. Rev.* **2011**, *40*, 1697.
11. Choi, C. H.; Park, S. H.; Woo, S. I. *Phys. Chem. Chem. Phys*. **2012**, *14*, 6842.
12. Ganguly, A.; Anjaneyulu, O.; Ojha, K.; Ganguli, A. K. *Cryst. Eng. Comm.* **2015**, *17*, 8978.
13. Mao, Y.; Park, T. J.; Wong, S. S. *Chem Commun*. **2005**, *46*, 5721.
14. Gulden, C.; Suleyman, C. *Cent. Eur. J. Phys.* **2013**, *11*, 387.
15. Ohkoshi, S.; Tsunobuchi, Y.; Matsuda, T.; Hashimoto, K.; Namai, A.; Hakoe, F.; Tokoro, H. *Nat. Chem.* **2010**, *2*, 539.
16. Sevincli, H.; Topsakal, M.; Durgun, E.; Ciraci, S. *Phys. Rev. B* **2008**, *77*, 195434.
17. Osaka, T.; Sayama, J. *Electrochim. Acta* **2007**, *52*, 2884.
18. Sun, L.; Zhang, R.; Wang, Z.; Ju, L.; Cao, E.; Zhang, Y. *J. Magn. Magn. Mater*. **2017**, *421*, 65.
19. Das, B. B.; Ramesh, S. *AIP Conf. Proc.* **2008**, *1003*, 85.
20. Opuchovic, O.; Kareiva, A.; Mazeika, K.; Baltrunas, D. *J. Magn. Magn. Mater*. **2017**, *442*, 425.
21. Yue, Z.; Li, L.; Zhou, J.; Zhang, H.; Gui, Z. *Mater. Sci. Eng*. **1999**, *B 4*, 69.
22. Epifani, M.; Melissano, E.; Pace, G.; Schioppa, M. *J. Eur. Ceram Soc*. **2007**, *27*, 115.
23. Roisnel, T.; Carvajal, J.R. *Mater. Sci. Forum* **2001**, *378*,

118.
24. Patterson, A. L. *Phys. Rev.* **1939**, *56*, 978.
25. Jayswal, M. S.; Kanchan, D. K.; Sharma, P.; Gondaliya, N. *Mater. Sci. Eng. B* **2013**, *178*, 775.
26. Das, B. B.; Rao, R. G. *Phys. Status Solidi B* **2015**, *252*, 2680.
27. Ballhausen, C. J. *Introduction to Ligand Field Theory;* McGraw Hill Book Company Inc.: New York, 1966; p 258.
28. Figgis, B. N. *Introduction to Ligand Fields, 1st ed*. Wiley Eastern Limited: New Delhi, 1976; p 21.
29. Tauc, J.; Grigorovici, R.; Vancu, A. *Phys. Status Solidi B* **1966**, *15*, 627.